Paraglider flight logs as hypsometers: daily temperature profiles of an Alpine valley, its diurnal heating, and the nearly level ceiling of thermals

Jörg Korner

Independent researcher, Switzerland
joergkorner@gmail.com
ORCID: https://orcid.org/0009-0001-9201-7509

Preprint statement

This manuscript is a non-peer reviewed preprint submitted to EarthArXiv.

This is version 2 of the preprint (19 October 2026). Compared with version 1 (16 October 2026), the quality screening of the flight logs was tightened and the analyses were recomputed independently; the numbers differ accordingly, the conclusions do not. Hourly profiles, pointwise terrain screening and a discussion of flight-path effects were added.

The manuscript has been submitted for publication in the *Quarterly Journal of the Royal Meteorological Society*. Subsequent versions of this manuscript may have slightly different content. If accepted, the final version will be available via the "Peer-reviewed Publication DOI" link on this page.

Companion paper: J. Korner, Paragliders as probes of the Alpine boundary layer: sink polars from 86 000 flight logs and the flow field of a valley, EarthArXiv, https://doi.org/10.31223/X5G23K.

Licence

CC BY 4.0 (Creative Commons Attribution).

Data and code availability

The derived data (layer estimates of every retained flight with an anonymous flight key, daily and hourly profiles, terrain-masked retrievals, thermal tops, the Payerne soundings as used), the analysis scripts and the aggregate tables behind every number of the paper are archived at Zenodo, version 2, https://doi.org/10.5281/zenodo.23474337. Version 1 of the archive remains available at https://doi.org/10.5281/zenodo.23418086. The flight logs were provided by XContest and cannot be redistributed; no pilot is identified.

Paraglider flight logs as hypsometers: daily temperature profiles of an Alpine valley, its diurnal heating, and the nearly level ceiling of thermals

Jörg Korner
Independent researcher, Switzerland
joergkorner@gmail.com

19 October 2026

Short title: Paraglider flight logs as hypsometers

Abstract

A paraglider flight recorder stores both pressure and GNSS altitude: together they turn routine flight logs into hypsometric measurements of layer-mean virtual temperature. From 86 369 IGC logs of the Valais, Swiss Alps, quality screening retains 13 520 dedicated-instrument flights on 437 days in 2011–2026; 392 days provide at least one profile layer supported by ten flights. At midday, between about 2200 and 3600 m, the profiles differ from the Payerne radiosonde, 100 km away, by a median of +0.67 K with a scaled median absolute deviation of 1.47 K (1545 layer comparisons on 370 days). Between morning (07–10 UTC) and afternoon (14–18 UTC), temperatures increase by 3.6 K near 2200 m (95 % interval 3.0–4.1 K) and 1.7 K near 3020 m (1.3–2.2 K). Hourly estimates resolve the daytime increase, and pointwise removal of fixes within 300 m of terrain preserves it. On matched observing days, median changes in the humidity contribution at Payerne are only a few tenths of a kelvin, supporting a predominantly thermal interpretation of the multi-kelvin valley signal. The upper envelope of 53 320 observed climbs follows terrain by factors of only 0.2–0.3 at scales of 2.5–10 km. A hydrostatic thought experiment explains how flight geometry can suppress a local warm-slope signal and motivates a comparison of slope-following and slope-leaving climbs. Routine flight archives thus provide a repeatable, vertically resolved record of daytime valley warming without additional airborne sensors.

Keywords: paraglider flight logs; hypsometer; temperature profiles; thermals; Alpine valley; convective boundary layer; mountain meteorology; crowdsourced observations

1 Introduction

Recreational paragliders sample the convective boundary layer of the Alps for hours on many flying days. Their logs, uploaded to online contests, provide a spatially extensive but selective record: weather, pilot decisions and flight access determine where and when observations exist. A companion paper (Korner, 2026b) read the vertical motion of the air from these logs, after deriving the sink polars of the gliders from the logs themselves. This paper reads their temperature, with a method that needs nothing beyond what the logs contain, tests it against a radiosonde on hundreds of days, and uses it for two questions about the mountain boundary layer on which campaigns and models disagree.

The convective boundary layer over mountains is poorly observed (Rotach and Zardi, 2007; Serafin et al., 2018; Lehner and Rotach, 2018). Routine radiosonde networks provide limited

coverage inside mountain valleys, while dedicated campaigns resolve processes over shorter periods. The relationship between local thermal structure and the valley-scale boundary layer remains an active question. De Wekker and Kossmann (2015), reviewing the concepts, describe a boundary-layer top that follows the terrain in the morning and may become level in the afternoon when the valleys heat fast enough, and note that detailed observations of this structure are still limited; airborne lidar over the Alps found aerosol layers that did not follow the topography (Nyeki et al., 2000), and soundings in deep Alpine valleys show a mixed layer growing to about the height of the surrounding ridges in the afternoon (Chemel and Chollet, 2006). How strongly the elevated terrain heats the atmosphere in place is a related question: a valley warms more than the plain for the same sunshine because it has less air to heat per unit of surface (Steinacker, 1984; Whiteman, 2000; Wagner et al., 2015), and the heating drives the slope and valley winds and the export of valley air to the free troposphere (Henne et al., 2004; Schmidli, 2013; Leukauf et al., 2016). Numbers for these processes come from a handful of campaigns such as the Riviera project (Rotach et al., 2004), and from models (Weigel et al., 2006; Leukauf et al., 2016).

The measurement rests on a property of the logs that needs no polar and no segmentation: most flight recorders write two altitudes, one from a barometer and one from a GNSS receiver. The two together can estimate virtual temperature layer by layer under the assumptions of the hypsometric equation, in the same way that Stone and Kitchen (2015) and de Haan (2026) extract temperature and humidity from the altitude reports of airliners, whose surveillance messages have long been turned into temperature and wind observations (de Haan, 2011). A paraglider does this at 1–2 $\mathrm{m\,s^{-1}}$ of vertical speed, along slopes and over valleys, for hours, and on a good day hundreds of them do it at once. Tracks recorded for other purposes are increasingly read as atmospheric observations: the GPS tracks of soaring birds for wind and thermals (Treep et al., 2016), smartphone barometers for surface pressure (Mass and Madaus, 2014), and the logs of competition sailplanes for the structure of thermals (Ultsch, 2012).

Temperature profiling from geometric and pressure altitude has precedents in aircraft surveillance data (de Leege et al., 2013; Stone and Kitchen, 2015). Instrumented paragliders have also measured temperature and humidity directly (Coppola, 2021), flight trajectories have supported empirical convection modelling (Pálenik et al., 2021), while large flight-log studies have characterised thermal ceilings, strength and variability (Hernández-Aguayo et al., 2026), and evaluated thermal forecasts (Nardon et al., 2026). Dedicated valley campaigns such as CROSSINN combine soundings, aircraft and remote sensing to resolve atmospheric structure (Adler et al., 2021). The contribution here is to turn the paired altitudes already present in routine paraglider archives into repeated valley-temperature profiles. To our knowledge, this is the first demonstration of daily and hourly hypsometric temperature profiling of an Alpine valley from a large archive of routine paraglider flight logs. It extends the observational record across hundreds of flying days, with no additional airborne temperature sensor.

The paper shows the method, its agreement with a geographically separated radiosonde and the checks that a flight is a usable hypsometer (Sections 2–4) and then uses the profiles and the thermals of the same logs for two questions: how much the valley atmosphere warms over the day, by height (Section 5), and whether the ceiling of the thermals follows the terrain (Section 6). Section 7 discusses flight-path effects and the observational coverage of the profiles.

2 Data and method

2.1 Flight logs

The source dataset contains 86 369 IGC flight logs of the Valais, 2007–2026, provided by XContest (XContest, 2026) under a confidentiality agreement; no raw log is redistributed and no pilot

is identified. Instrument screening identifies 31 677 logs from dedicated flight instruments with distinct pressure and GNSS altitudes. Excluding smartphone applications and unnamed instruments, and requiring at least 20 candidate flights per day, gives 14 918 candidate logs on 437 days from 2011 onwards.

Quality control removes 22 duplicate recordings with identical B-record position and altitude sequences, retains valid fixes with strictly increasing timestamps, and requires at least 300 retained fixes per flight. Flights lie entirely inside the terrain mosaic (45–47° N, 6–9° E). The resulting 13 520 flights provide eligible layer estimates on 437 days, of which 392 meet the ten-flight threshold for at least one broad-window layer. Sample sizes are reported separately for each contrast. The thermal-ceiling analysis uses the climb-selection criteria described in Section 2.4.

2.2 Layer temperature from two altitudes

Pressure altitude z_p is inverted using the standard-atmosphere relationship, $p = 1013.25(1 - 2.25577 \cdot 10^{-5} z_p)^{5.25588}$ hPa. For a hydrostatic column, the local hypsometric relationship is

$$T_v = -\frac{g}{R_d}\left(\frac{\partial \ln p}{\partial z}\right)^{-1}, \tag{1}$$

with $g = 9.80665\,\mathrm{m\,s^{-2}}$ and $R_d = 287.05\,\mathrm{J\,kg^{-1}\,K^{-1}}$. Within each flight, time window and 25-hPa layer between 875 and 525 hPa, GNSS altitude is regressed on $\ln p$ and the slope is multiplied by $-g/R_d$. This is an effective layer estimate along the sampled path; its equality to a local column temperature requires horizontal and temporal pressure variations to be negligible or suitably controlled (Section 7). GNSS geometric height is used as an approximation to geopotential height.

The broad windows are 07–10, 10–14 and 14–18 UTC. Each flight-window must contain at least 100 fixes, and each layer regression at least 40 fixes spanning at least 15 hPa. A profile value for each day, window and layer is the median across flights, with at least ten contributing flights. A constant additive GNSS-height offset cancels in the slope. A constant additive pressure error does not cancel exactly: if $p_m = p + b$ in a vertical isothermal column, the inferred local temperature is multiplied by $(p + b)/p$. Similarly, a constant pressure-altitude offset is not an exactly constant $\ln p$ offset after the nonlinear inversion. Time-dependent calibration, pressure changes and horizontal gradients can also affect the slope. No general cancellation of barometric errors is assumed.

The measured thermodynamic variable is virtual temperature, $T_v \simeq T(1 + 0.608q)$ for unsaturated air, where T is air temperature in kelvin and q is specific humidity in $\mathrm{kg\,kg^{-1}}$. This is the temperature variable entering the hydrostatic equation. We use "hypsometric temperature" for this measurement and retain T_v in equations and quantitative comparisons. Changes satisfy $\Delta T_v = \Delta T + \Delta(T_v - T)$. Section 5.1 quantifies the second term at Payerne to assess its regional scale. Sampling uncertainty and systematic sensitivities are evaluated in Section 4.

2.3 Instruments

Instrument diagnostics use samples selected for the comparisons below, including smartphone and pre-2011 records. They are distinct from the sample used for the temperature profiles.

Recalibration. Some instruments continuously adjust their barometric altitude to the GNSS altitude. Their layer temperatures reproduce the standard atmosphere whatever the real air. A flight-window with at least two layer estimates is flagged when the absolute median difference from the standard atmosphere is below 1.5 K. This is a temperature-dependent screening

heuristic, not an independent identification of recalibration. For all terrain masks and hourly retrievals, the flag is inherited from the unmasked broad window, preventing the filter from being retuned separately to each result. Sensitivity to omitting the rule is reported with the analysis tables. Without the rule, the morning-to-afternoon increase at 787.5 hPa is 3.68 K (95 % interval 3.28–4.38 K; 112 days) instead of 3.55 K, and the median difference from Payerne is +0.57 K (1621 comparisons) instead of +0.67 K; the rule removes 6.03 % of eligible broad-window flight segments.

Thermal lag of smartphones. For smartphone logs the difference between the two altitudes drifts during fast climbs, consistent with a barometer that follows the temperature of the phone rather than the air. Smartphone logs are therefore left out.

Early instruments. Profiles from 2008–2010, when the first generation of flight instruments dominated, lie 2–5 K below the radiosonde (medians −4.7, −3.6 and −2.1 K); from 2011 on the difference is stable between +0.2 and +1.5 K in every year. All results use 2011–2026.

2.4 Thermals

For Section 6, climbs were identified in the same logs as contiguous circling (heading change of more than 60° within a centred 20-s window) of at least 120 s with at least 150 m of height gain, the vertical velocity of the air being the barometric vertical speed smoothed over 15 s plus a constant sink of the glider of 1.3 m s^{-1}. This is a simpler rule than the segmentation of the companion paper and is sufficient here, since only the top height of each climb is used. Between 10 and 16 UTC it finds 54 481 thermals on 401 days from 2011 on. Days on which the thermal tops pile up at one height (95th minus 70th percentile of the tops below 150 m: cloud base or an airspace limit) are excluded, 15 days, leaving 53 320 thermals on 386 days.

2.5 Use of AI tools

The author conceived the study, obtained the data, designed the analyses and interpreted the results. AI assistants (Claude, Anthropic; Codex, OpenAI) were used as programming aids, for an independent recomputation of the temperature analysis from the raw logs and of the thermal-ceiling analysis from the archived derived data, which reproduced the original results before the quality screening was tightened, and for language editing. The author checked all results and takes full responsibility for the content.

3 Comparison with the Payerne radiosonde

Payerne (491 m, on the Swiss Plateau, about 100 km from the centre of the Valais) launches radiosondes at 00 and 12 UTC. The IGRA2 data (Durre et al., 2018) supply virtual temperatures averaged over the same 25-hPa layers. We compare the 10–14 UTC profiles with the 12 UTC sounding on 381 days, giving 2297 layer comparisons.

Between approximately 2200 and 3600 m (layer centres 787.5–662.5 hPa), the median flight-minus-sonde difference is +0.67 K and its scaled median absolute deviation is 1.47 K across 1545 comparisons on 370 days (Fig. 1). The scaled MAD is 1.4826 median$|x - \text{median}(x)|$ and describes dispersion; it is not a confidence interval or a median standard error.

The lower-layer positive differences are consistent with enhanced daytime temperatures over the valley. Because Payerne samples a different location and potentially a different air mass, this comparison measures regional agreement rather than local absolute accuracy. The within-day contrasts below test the valley's daytime evolution independently of this spatial

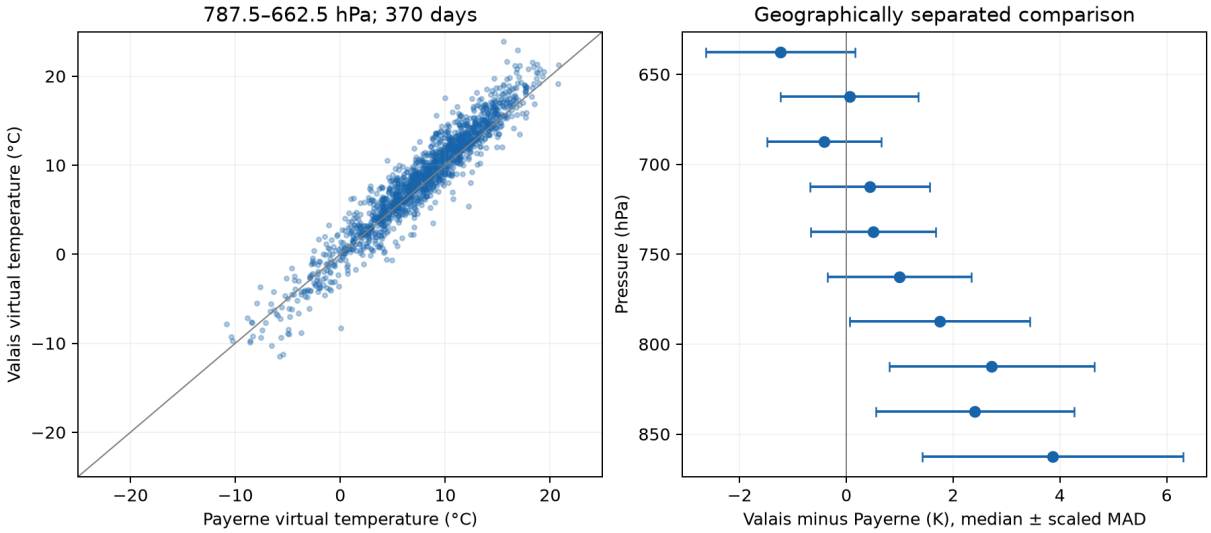


Figure 1: Quality-screened flight estimates compared with Payerne at 12 UTC. Left: layer temperatures at 787.5–662.5 hPa. Right: median difference and scaled MAD by layer. Differences combine instrumental, sampling and geographical effects.

difference, and the humidity analysis assesses the magnitude of the regional moisture contribution.

4 Uncertainty and robustness checks

4.1 Sampling uncertainty and dependence

Sampling errors of daily/window/layer medians are obtained by bootstrapping whole flight estimates (999 replicates), rather than individual fixes (Hesterberg, 2015). Across 4114 eligible groups, the median standard error is 1.34 times scaled-MAD/$\sqrt{n}$, showing the importance of estimating the sampling uncertainty of the median directly. A second bootstrap resamples 5-km spatial cells combined with integer UTC hours, retaining the associated flights together. Across 4010 groups with at least five blocks, its median standard-error ratio to the flight bootstrap is 1.00.

Time-window contrasts are paired within day and layer before resampling days (2000 replicates). Calendar-week blocks provide a further dependence check and preserve the principal warming signals. Reported intervals are pointwise 95 % sampling intervals; instrument and sampling sensitivities are assessed separately. Sparse cases are identified by their sample sizes.

4.2 Instrument and sampling sensitivities

Instrument-family comparisons on dedicated-instrument logs before the fix-level quality filters give differences of approximately 1.1 K between grouped families, with different absolute offsets against Payerne. A fixed family offset can cancel in a within-day contrast only insofar as the contributing instruments and their errors remain comparable. We therefore additionally compare hours or broad windows within the same day, pressure layer, approximately 10-km cell and instrument family, requiring at least two flights per cell-family-window. Cell-family contrasts are reduced to one median per day before resampling days. These controls reduce geographical and family-composition differences but do not remove within-family calibration drift or guarantee equal spatial sampling.

A climb/sink comparison on the same diagnostic dataset gives midday differences of about −0.23 K. It remains a useful complementary diagnostic of direction-dependent errors, without proving that pressure tendency or sensor drift has been uniquely separated. No single offset such as ±0.5 K is treated as a comprehensive systematic-error bound.

4.3 Pointwise exclusion near terrain

The terrain mask is applied to individual fixes *before* each regression. SRTM 3-arc-second terrain (Farr et al., 2007) is searched within horizontal radii of 100, 300, 600, 1000 and 1500 m for terrain reaching at least the GNSS flight height minus 50 m. The operational distance is therefore horizontal distance to terrain of similar elevation, not slope-normal distance. Tests use approximately 64-m east–west and 92.6-m north–south grid spacing. All terrain-selected fixes must have non-negative height above valid terrain. The strict free-air mask also requires more than 500 m above ground. Grid resolution and GNSS/geoid differences limit interpretation of the 100-m class.

After masking, each regression must still contain at least 40 fixes spanning 15 hPa. Profiles are compared on the same dates, windows and layers. A second diagnostic pairs the masked and unmasked retrievals from the same flights, separating retrieval changes from changes in flight selection. All masks use the same recalibration flags.

At 787.5 hPa (about 2200 m), removing fixes within 300 m of terrain leaves a morning-to-afternoon increase of 3.20 K (95 % interval 2.57–4.00 K; 74 days). The paired change of warming relative to the unmasked result on exactly those days is -0.06 K (-0.33 to +0.21 K; 74 days). The warming is therefore not explained by the inclusion of the nearest-terrain fixes in this sample. Stricter exclusion is much more costly: the free-air selection retains only one paired day at 787.5 hPa, compared with 12 at 762.5 hPa and 35 at 712.5 hPa. Consequently it cannot establish lower-layer morning robustness. The latter two free-air warming estimates are 2.85 K (95 % interval 2.07–3.99 K; 12 days) and 1.67 K (95 % interval 1.03–2.24 K; 35 days), respectively.

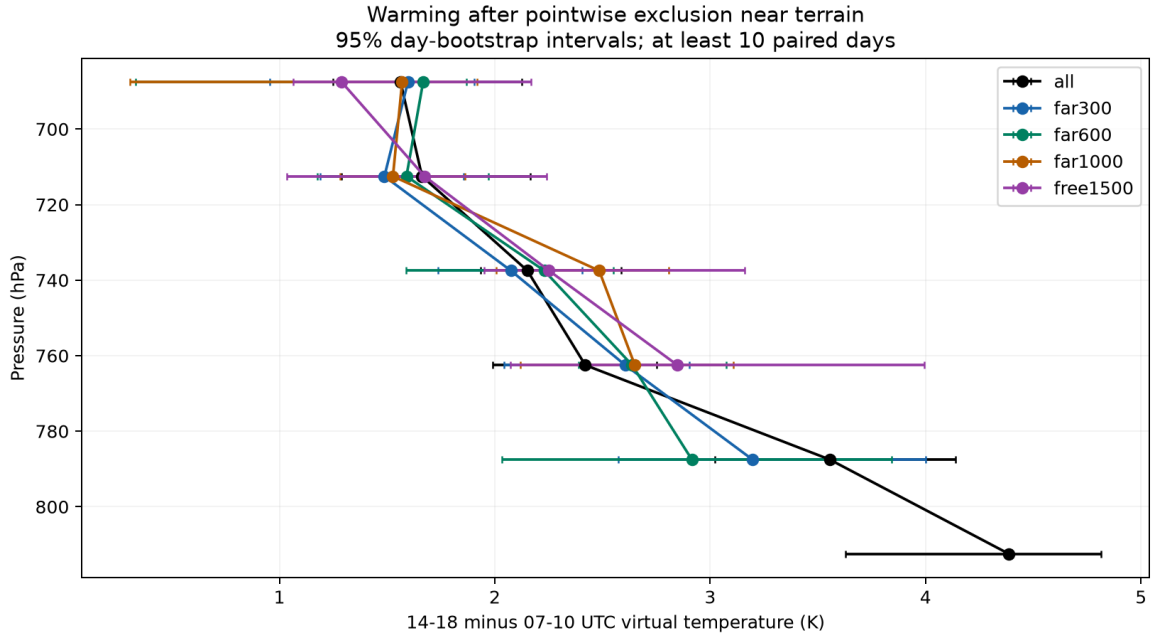


Figure 2: Morning-to-afternoon virtual-temperature changes after pointwise terrain exclusion. Each curve uses dates with at least ten flights in both windows for its mask; different masks therefore have different date sets. Intervals resample paired daily differences. Matched-date changes are reported separately in the text and tables. Only groups with at least ten paired days are plotted. "far300/600/1000" denote the exclusion radius in metres; "free1500" additionally requires 500 m above ground.

Near-only versus free-only comparisons also remain sampling limited. At 762.5 hPa at mid-day, the near-100-m minus free-air contrast is -0.35 K (-1.61 to +0.05 K; 27 days). This comparison resolves no clear positive near-slope temperature excess. It does not establish the temperature of a local slope layer, because the two samples also differ in their locations and flight paths. Section 7 develops a physical explanation for the sign and a flight-path comparison to test it.

5 Observed diurnal evolution

The broad-window estimates show morning-to-afternoon virtual-temperature increases of 4.39 K (95 % interval 3.63–4.82 K; 28 days) at approximately 1940 m, 3.55 K (95 % interval 3.02–4.14 K; 107 days) at 2200 m, 2.42 K (95 % interval 1.99–2.75 K; 108 days) at 2470 m, 2.15 K (95 % interval 1.93–2.59 K; 86 days) at 2740 m and 1.66 K (95 % interval 1.29–2.16 K; 45 days) at 3020 m. These are medians of 14–18 minus 07–10 UTC contrasts within individual days. Their intervals express sampling uncertainty across the observed flying days, not all-weather climatological uncertainty.

Hourly regressions use the same pressure spans and minimum numbers of fixes; each hourly profile still requires ten flights. Figure 3 compares each observed hour with 10–11 UTC on the same dates. At 787.5 hPa the median contrasts are -2.02 K at 08–09 UTC (23 paired days), -1.03 K at 09–10 UTC (61), +0.92 K at 11–12 UTC (46), +1.31 K at 12–13 UTC (56), +2.44 K at 13–14 UTC (49), +2.38 K at 14–15 UTC (48) and +2.97 K at 15–16 UTC (27). Each point uses its available date intersection with the reference hour; it is not a single fixed-cohort trajectory. Restricting 09–16 UTC to the same complete dates leaves 14 days at 787.5 hPa and retains the rising evolution. The corresponding complete-date tables are supplied.

Matching the 10-km cell and instrument family retains a broad-window increase of 3.26 K (0.66–4.85 K; 63 days) near 2200 m. These controls reduce changes in spatial and instrument composition. Together with the fixed-date hourly comparison and pointwise terrain screening, they support a daytime warming signal extending beyond the nearest-slope measurements. The resolved evolution begins with the first sufficiently sampled hour; no extrapolation to dawn is required.

5.1 Humidity contribution on matched observing days

The Payerne soundings contain both T and T_v in the same pressure layers. We calculate $C = T_v - T$ for each sounding, then difference C within each paired date and layer. Only dates with both morning and afternoon Valais estimates and both relevant Payerne soundings are retained. This directly quantifies the moisture contribution to the Payerne temperature change. Table 1 gives medians and interquartile ranges for 00–12 UTC, alongside Valais contrasts on exactly those dates. Specific humidity inferred from the ratio of the layer-mean temperatures is an effective layer value, $q \simeq (T_v/T - 1)/0.608$; the correction C itself requires no such inversion.

Median moisture contributions range from -0.28 to -0.03 K for 00–12 UTC; the complementary 12–00 UTC next-day comparison gives $+0.05$ to $+0.22$ K. Thus the regional median moisture contribution is only a few tenths of a kelvin, compared with several kelvin of valley warming. This independent evidence supports a predominantly thermal interpretation of the observed signal. Payerne supplies a regional scale comparison, not a local humidity correction: its location and sounding intervals differ from those of the flights, and the median changes do not bound individual days or intermediate hours.

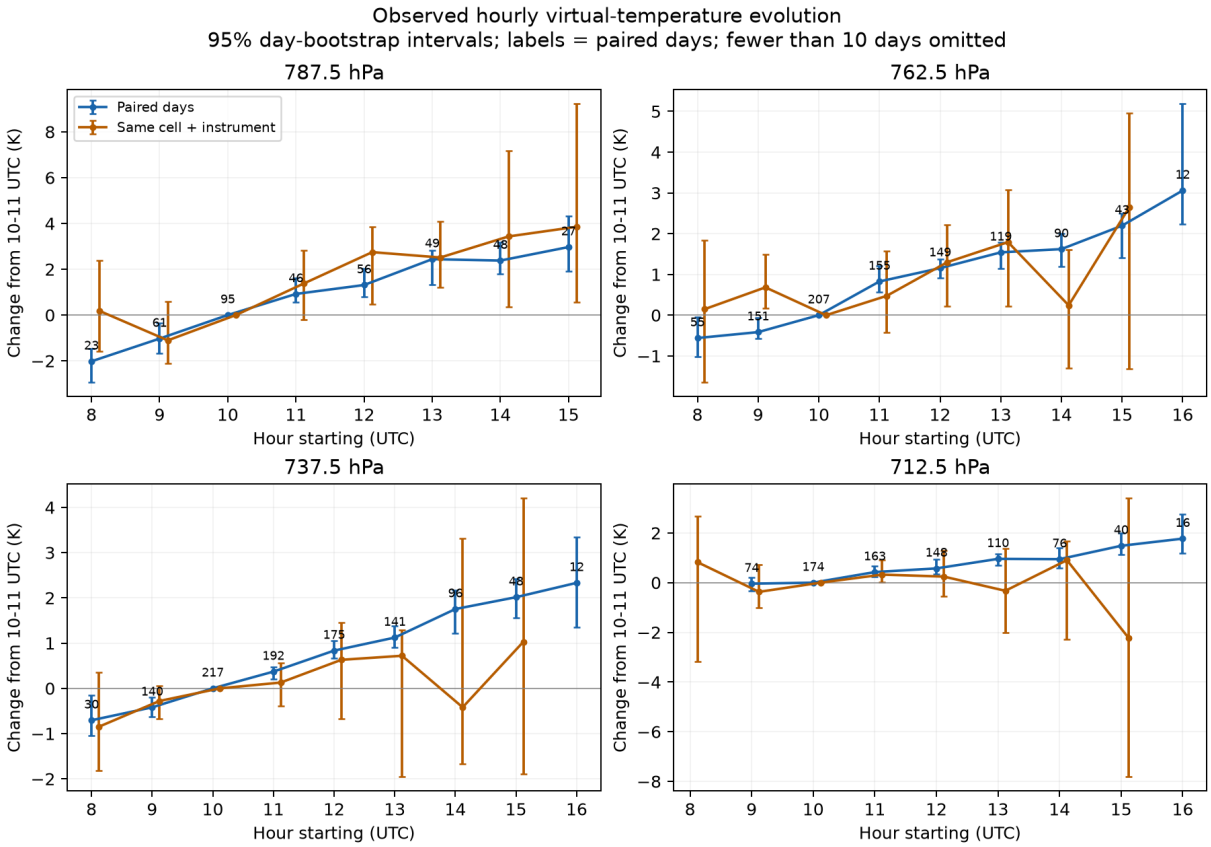


Figure 3: Observed hourly virtual-temperature contrasts relative to the measured 10–11 UTC hour, paired within days. Blue: profiles with at least ten flights per hour; labels give paired-date counts. Orange: additionally matched 10-km cell and instrument family, at least two flights in each cell-family-hour, summarised once per day. The orange and blue samples need not contain the same dates. Pointwise 95 % intervals resample days. Groups with fewer than ten dates are omitted. The reference hour is identically zero by construction.

Table 1: Payerne humidity contribution on dates with paired Valais morning and afternoon estimates. ΔC is the 12 minus 00 UTC change in $T_v - T$; brackets give the interquartile range across days, not a confidence interval. The last column gives the Valais 14–18 minus 07–10 UTC contrast on the same dates. Each entry is the median of paired differences.

Layer (hPa)	Days	Δq (g kg^{-1})	ΔC (K) [IQR]	Valais ΔT_v (K)
812.5	24	−1.64	−0.28 [−0.40, −0.05]	4.50
787.5	96	−0.76	−0.13 [−0.29, +0.07]	3.73
762.5	96	−0.36	−0.06 [−0.28, +0.08]	2.39
737.5	75	−0.72	−0.12 [−0.29, +0.06]	2.16
712.5	39	−0.13	−0.03 [−0.15, +0.11]	1.50

5.2 Column-equivalent warming energy

As a descriptive column-equivalent energy proxy, we compute

$$E^* = \frac{c_p}{g} \sum_{800\text{–}700\,\mathrm{hPa}} \Delta p \, \Delta T_v, \tag{2}$$

using $c_p = 1005\,\mathrm{J\,kg^{-1}\,K^{-1}}$, $\Delta p = 2500\,\mathrm{Pa}$ and only dates with paired estimates in all four layers. The median is $2.50\,\mathrm{MJ\,m^{-2}}$ (95 % sampling interval 2.41–2.95; 43 days; 4000 bootstrap replicates). Summing different layers' medians on different day sets is avoided. This proxy is not a measured valley-integrated heat-storage budget: virtual temperature includes humidity, the flight medians are not area-weighted means, pressure surfaces intersect mountain terrain, and advection and moving sampling volumes are not resolved. It is consistent in scale with substantial daytime warming, but does not close the heat budget discussed in mountain-boundary-layer studies (Rotach et al., 2004; Weigel et al., 2006; Schmidli, 2013).

6 The ceiling of thermals and the terrain

6.1 Thermals are left early

Only 2.5 % of the thermals are flown out, that is, left with a climb rate below $1\,\mathrm{m\,s^{-1}}$; the median climb rate at the moment of leaving is $2.0\,\mathrm{m\,s^{-1}}$. The height at which a thermal is left is therefore the pilot's decision, and the top of the lift is a lower bound. To see how much is missing, a remaining-climb function was learned from the flown-out thermals: each is cut artificially at the moment its climb rate first drops to 3.0, 2.5, 2.0 or $1.5\,\mathrm{m\,s^{-1}}$, and the height it still gained after that is recorded by the trend of the climb over the previous 300 m and the strength of the thermal. Learned on the flown-out thermals of half of the days and tested on the other half, the function predicts the remaining climb with a median error of +25 m and a spread of 150 m. Of the 51 978 thermals left early, 18 680 gained less than 325 m, too little for the trend over the last 300 m, and keep their observed top; of the 33 298 others, 10 655 fall in classes whose learned remaining climb is zero (the climb was already fading), and 22 643 receive a remaining climb, 225 m in the median (quartiles 150–475 m). The function is learned from the 2.5 % of thermals that pilots flew out, which may differ from the rest; this is the reason for treating the correction as a check and the observed top as the quantity.

6.2 Does the ceiling follow the terrain?

What is measured is the upper envelope of the observed climbs, called the ceiling here for brevity. It is a lower bound on the tops of the thermals themselves; whether those lie above or below the top of the mixed layer depends on its definition and on the overshoot of thermals into the stable air, which these data do not resolve. For each day and each cell of a grid of 2.5, 5 or 10 km with at least eight thermals, the ceiling is the 90th percentile of the thermal top heights, and the terrain height of the cell is the mean of the SRTM 3″ elevation (Farr et al., 2007). Within each day with at least four such cells, ceiling and terrain are expressed as deviations from the day's mean, so that the overall level of the day cancels, and the ceiling deviation is regressed on the terrain deviation over all days (Fig. 4). The 95 % intervals come from resampling the days. Within a day the terrain of the cells spans 750 m (2.5 km cells) to 1220 m (10 km) in the median, and the ceiling lies at 3230–3290 m.

The factor is 0.32 (95 % interval 0.23–0.42) at 2.5 km, 0.21 (0.15–0.28) at 5 km and 0.22 (0.17–0.25) at 10 km, from 925, 1399 and 1650 cell-days on 91, 143 and 184 days. A cell whose terrain

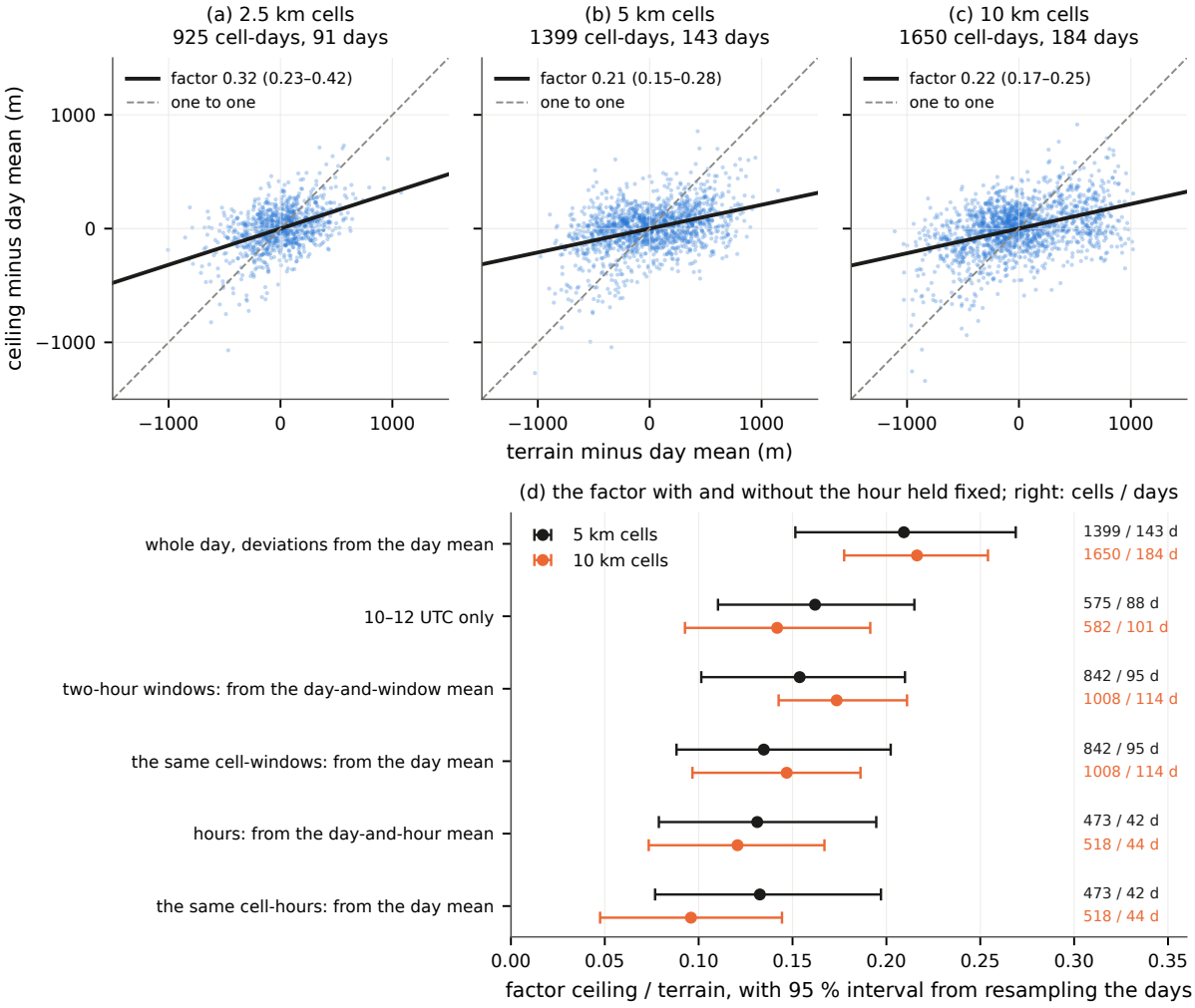


Figure 4: Ceiling of thermal lift against the terrain, within the same day. Each point is one cell on one day: the 90th percentile of the thermal tops in the cell, minus the day's mean over its cells, against the mean terrain height of the cell, minus the day's mean. (a)–(c) Cells of 2.5, 5 and 10 km. The line is the fit, with its factor and 95 % interval from resampling the days; the dashed line is a ceiling that follows the terrain one to one. (d) The factor for the whole day, for 10–12 UTC alone, and for the samples that allow the hour of the day to be held fixed: two-hour windows and single hours, each once with the deviations from the mean of the day and window or hour, and once, on exactly the same cells, from the mean of the day. Right: number of cell-days, cell-windows or cell-hours, and of days.

lies 1000 m above the day's mean has a ceiling 210–320 m higher, not 1000 m. With the remaining climb of Section 6.1 added to every thermal left early, the factors are 0.23 (0.18–0.29) at 5 km and 0.21 (0.17–0.26) at 10 km, against 0.20 and 0.21 for the same cell-days without it: this particular correction changes the fitted factor little on the matched sample; other selection effects remain possible. The direction of any remaining selection bias cannot be established from these data alone.

The cells of a day are not all flown at the same hour, and the ceiling rises during the day, so the factor could contain a time-of-day effect. Within a day the ceiling rises by 77 m per hour (90th percentile of the tops per day and hour, 773 day-hours on 169 days; -170 m at 10 UTC, $+200$ m at 15 UTC relative to the day's mean), and the thermals over the lowest cells are flown 0.4–1.1 h later than those over the highest (12.3–12.5 h against 11.4–11.9 h). This gives the lowest cells a late-day bonus of 33–85 m, which lowers the apparent factor by at most 0.03–0.08; a correction for the hour should raise it slightly. Figure 4d shows the test. Taking cell-hours with at least eight thermals in the hour and at least four cells per day and hour, the factor from the deviations from the mean of the day and hour is 0.13 (0.08–0.19) at 5 km and 0.12 (0.07–0.17) at 10 km, from 473 and 518 cell-hours on 42 and 44 days; from the deviations from the day mean, on exactly the same cell-hours, it is 0.13 (0.08–0.20) and 0.10 (0.05–0.14). With two-hour windows (10–12, 12–14, 14–16 UTC) it is 0.15 (0.10–0.21) and 0.17 (0.14–0.21) from 842 and 1008 cell-windows on 95 and 114 days, against 0.13 (0.09–0.20) and 0.15 (0.10–0.19) on the same cell-windows from the day mean; within 10–12 UTC alone it is 0.16 (0.11–0.21) and 0.14 (0.09–0.19). Holding the hour fixed thus changes the factor by $+0.00$ to $+0.02$, the direction and size expected from the rise of the ceiling; the lower values of the hourly samples against the day-wide 0.21–0.22 come from the cells and days these samples select, the busy ones, not from the hour.

The upper envelope of the climbs over the Valais between 10 and 16 UTC is therefore nearly level, with a slight doming over high terrain, on all scales from 2.5 to 10 km: a factor of 0.2–0.3 across the day, 0.10–0.17 in the samples that allow the hour to be held fixed, and less than 0.1 of it from the hour. This is the afternoon state that De Wekker and Kossmann (2015) describe as reached when the valleys heat fast enough, and it is consistent with the lidar observations of Nyeki et al. (2000); here it is measured on 184 days. The flight-top envelope and the Payerne comparison do not uniquely identify the physical mixed-layer top. The thermal ceiling is one of the three observables that Hernández-Aguayo et al. (2026) relate to reanalysis predictors over France; the present analysis quantifies its relationship to terrain within the same day.

7 What a hypsometer flown along a slope measures

Under hydrostatic balance, pressure measures the weight of the air column overhead per unit area. The hypsometric method uses the height difference between pressure levels to measure the temperature of the intervening air: warm air occupies a greater depth for the same pressure ratio. A vertical climb samples successive levels of one column. A climb along a slope also moves between columns. The pressure differences between those columns can reinforce or offset the signal from the warm air through which the pilot flies.

Consider a thin warm layer lying along a planar slope. To isolate the effect of flight geometry, suppose that the layer is stationary, its temperature excess depends only on distance normal to the slope, the background temperature is constant, and pressure approaches the same background atmosphere well above the layer. These assumptions specify a simple hydrostatic thought experiment. A pilot climbing vertically moves out through the warm layer, and the pressure change with height records its elevated temperature. A pilot climbing parallel to the slope at constant distance remains at the same position within the warm-layer structure.

In the parallel case, the warm air overhead produces the same proportional pressure deficit relative to the background at each point along the climb. This constant proportion cancels when the pressure ratio between two points is taken. The retrieved temperature therefore equals the background temperature, even though the pilot encounters warmer air. The important condition is the unchanged proportional pressure deficit along the path, rather than proximity to terrain alone. This example shows how a warm layer can escape a hypsometric measurement along a particular path. It specifies a pressure field in vertical hydrostatic balance; it does not describe the full circulation driven by the layer or imply that real slope layers are generally invisible.

A changing pressure deficit gives a second possibility. If the proportional deficit becomes larger as the pilot climbs, pressure falls more rapidly along the path than it does in the background atmosphere. The retrieval then gives a lower temperature, even when the air encountered is warm. An increase in the strength of the warm layer uphill can produce this behaviour under the same upper-pressure condition. A weakening deficit has the opposite effect. Layer growth during the flight, changes in thickness and departures from a slope-parallel path must therefore be assessed through their effect on the pressure field; warming near the ground alone does not determine the sign of the retrieved anomaly.

This gives a physical interpretation to test against the near-slope observations. At 762.5 hPa, the midday near-100-m minus free-air contrast is -0.35 K (95 % interval -1.61 to $+0.05$ K; 27 days). Its sign is consistent with a pressure deficit strengthening along an ascending path. The interval includes zero, however, and the two samples differ in location and flight geometry; variable slope-layer temperatures and GNSS errors near terrain can also contribute. The contrast therefore motivates the mechanism as a hypothesis. Establishing it requires knowing whether a warm layer was present and how the sampled paths crossed its pressure field.

The logs provide a concrete way to investigate this hypothesis: compare climbs that leave a slope approximately vertically with climbs that follow it at nearly constant normal distance, matched in location, height, time and instrument. In the stationary uniform-layer example, the former detect warmth and the latter return the background temperature; a strengthening pressure deficit can make the latter appear cooler. This comparison requires slope-normal distance and path orientation at individual fixes. The horizontal terrain-distance mask used here does not by itself identify these paths. Colocated temperature and pressure observations would establish the actual warm-layer anomaly and test whether the predicted contrast occurs.

The existing terrain-exclusion test answers the broader observational question. Near 2200 m, removing fixes within 300 m of terrain preserves the morning-to-afternoon warming; on matched dates the change is only -0.06 K (95 % interval -0.33 to $+0.21$ K). Together with the cell-and-instrument controls, this shows that the daytime signal extends beyond the nearest-slope measurements. Its persistence does not depend on adopting the slope-layer explanation.

Coverage sets another limit. Pilots rarely sample stable air above the thermal ceiling, and the highest midday profile layer typically lies below the observed thermal tops. The profiles therefore describe the sampled valley atmosphere; they do not determine the unsampled stratification above the climbs or the overshoot of thermals into it.

8 Conclusions

Routine paraglider flight archives provide a new observational record of valley temperature. Paired pressure and GNSS altitudes yield daily profiles over hundreds of flying days and hourly contrasts that resolve the daytime evolution. The Valais measurements show a morning-to-afternoon increase of 3.55 K near 2200 m and 1.66 K near 3020 m. The signal persists after

pointwise removal of near-terrain fixes and after matching spatial cells and instrument families. Bootstrap intervals quantify its sampling uncertainty.

The median humidity contribution in matched Payerne soundings is a few tenths of a kelvin, supporting a predominantly thermal interpretation of the multi-kelvin valley changes. Midday agreement with this regional reference and the within-day controls provide complementary evidence. The 800–700-hPa column-equivalent warming proxy is 2.50 MJ m^{-2}; interpreting it as a valley heat-storage budget would additionally require local humidity and spatial weighting.

The upper envelope of observed climbs rises by only 210–320 m per 1000 m of terrain at 2.5–10 km scales, describing a nearly level thermal ceiling. The terrain-exclusion tests establish the persistence of daytime warming beyond the nearest-slope measurements. A hydrostatic thought experiment shows how a uniform warm layer can cancel from a slope-parallel retrieval when its proportional pressure deficit remains constant along the path. A deficit that strengthens along the climb can instead produce a negative retrieved anomaly. The observed near-slope contrast motivates a test of this mechanism using slope-following and slope-leaving climbs with colocated observations. The approach opens existing recreational-flight archives to repeated measurements of mountain-atmosphere thermal structure.

Data and code availability. The derived data, scripts and aggregate tables of the analyses presented here are archived at Zenodo (Korner, 2026a). Raw IGC logs remain confidential; reproducing the pointwise analysis requires authorised access to them and the SRTM terrain tiles.

Acknowledgements. XContest provided the flight logs. The Payerne soundings are from IGRA2 (NOAA NCEI), the terrain from SRTM.

Funding. This work received no funding.

Conflict of interest. The author declares no conflict of interest.

Permission to reproduce material from other sources. No material from other sources is reproduced.

Author contributions. J. Korner: conceptualization, methodology, software, formal analysis, data curation, visualization, writing.

References

Bianca Adler, Alexander Gohm, Norbert Kalthoff, Nevio Babić, Ulrich Corsmeier, Manuela Lehner, Mathias W. Rotach, Maren Haid, Piet Markmann, Eckhard Gast, George Tsaknakis, and George Georgoussis. CROSSINN: A field experiment to study the three-dimensional flow structure in the inn valley, austria. *Bulletin of the American Meteorological Society*, 102(1): E38–E60, 2021. doi: 10.1175/BAMS-D-19-0283.1.

Charles Chemel and Jean-Pierre Chollet. Observations of the daytime boundary layer in deep Alpine valleys. *Boundary-Layer Meteorology*, 119(2):239–262, 2006. doi: 10.1007/s10546-005-9026-4.

Arianna Coppola. Analysis of airborne measurements from paragliders to detect thermal structures in the mountain atmospheric boundary layer. Master's thesis, Università di Bologna, 2021. URL https://amslaurea.unibo.it/id/eprint/23468/.

Siebren de Haan. High-resolution wind and temperature observations from aircraft tracked by Mode-S air traffic control radar. *Journal of Geophysical Research*, 116:D10111, 2011. doi: 10.1029/2010JD015264.

Siebren de Haan. Upper air humidity from automatic aircraft surveillance data. EGUsphere preprint egusphere-2026-717, 2026. URL https://doi.org/10.5194/egusphere-2026-717.

A. M. P. de Leege, M. M. van Paassen, and M. Mulder. Using automatic dependent surveillance-broadcast for meteorological monitoring. *Journal of Aircraft*, 50(1):249–261, 2013. doi: 10.2514/1.C031901.

Stephan F. J. De Wekker and Meinolf Kossmann. Convective boundary layer heights over mountainous terrain: a review of concepts. *Frontiers in Earth Science*, 3:77, 2015. doi: 10.3389/feart.2015.00077.

Imke Durre, Xungang Yin, Russell S. Vose, Scott Applequist, and Jeff Arnfield. Enhancing the data coverage in the Integrated Global Radiosonde Archive. *Journal of Atmospheric and Oceanic Technology*, 35:1753–1770, 2018. doi: 10.1175/JTECH-D-17-0223.1.

Tom G. Farr, Paul A. Rosen, Edward Caro, Robert Crippen, Riley Duren, Scott Hensley, Michael Kobrick, Mimi Paller, Ernesto Rodriguez, Ladislav Roth, David Seal, Scott Shaffer, Joanne Shimada, Jeffrey Umland, Marian Werner, Michael Oskin, Douglas Burbank, and Douglas Alsdorf. The Shuttle Radar Topography Mission. *Reviews of Geophysics*, 45:RG2004, 2007. doi: 10.1029/2005RG000183.

Stephan Henne, Markus Furger, Stephan Nyeki, Martin Steinbacher, Bruno Neininger, Stephan F. J. De Wekker, Josef Dommen, Nicole Spichtinger, Andreas Stohl, and André S. H. Prévôt. Quantification of topographic venting of boundary layer air to the free troposphere. *Atmospheric Chemistry and Physics*, 4:497–509, 2004. doi: 10.5194/acp-4-497-2004.

César Hernández-Aguayo, Matthieu Cristelli, and Michael Benzaquen. From flight logs to atmospheric science: Paragliders as convection sensors for identifying thermal predictors. arXiv preprint, version 2, 2026. URL https://doi.org/10.48550/arXiv.2608.00241.

Tim C. Hesterberg. What teachers should know about the bootstrap: Resampling in the undergraduate statistics curriculum. *The American Statistician*, 69(4):371–386, 2015. doi: 10.1080/00031305.2015.1089789.

Jörg Korner. Paraglider flight logs as hypsometers: derived data and code. Zenodo, version 2, 2026a. URL https://doi.org/10.5281/zenodo.23474337.

Jörg Korner. Paragliders as probes of the Alpine boundary layer: sink polars from 86 000 flight logs and the flow field of a valley. EarthArXiv preprint, 2026b. URL https://doi.org/10.31223/X5G23K.

Manuela Lehner and Mathias W. Rotach. Current challenges in understanding and predicting transport and exchange in the atmosphere over mountainous terrain. *Atmosphere*, 9(7):276, 2018. doi: 10.3390/atmos9070276.

Daniel Leukauf, Alexander Gohm, and Mathias W. Rotach. Quantifying horizontal and vertical tracer mass fluxes in an idealized valley during daytime. *Atmospheric Chemistry and Physics*, 16:13049–13066, 2016. doi: 10.5194/acp-16-13049-2016.

Clifford F. Mass and Luke E. Madaus. Surface pressure observations from smartphones: a potential revolution for high-resolution weather prediction? *Bulletin of the American Meteorological Society*, 95(9), 2014. doi: 10.1175/BAMS-D-13-00188.1.

C. Nardon, E. Gambini, E. Maggioni, A. Perotto, R. Salerno, and A. Ceppi. Assessing WRF simulations for thermal forecasting in paragliding flights. *Meteorology and Atmospheric Physics*, 138:112, 2026. doi: 10.1007/s00703-026-01215-x.

Stephan Nyeki, Markus Kalberer, Ian Colbeck, Stephan De Wekker, Markus Furger, Heinz W. Gäggeler, Meinolf Kossmann, Matthias Lugauer, Douw Steyn, Ernest Weingartner, Martin Wirth, and Urs Baltensperger. Convective boundary layer evolution to 4 km asl over high-alpine terrain: airborne lidar observations in the Alps. *Geophysical Research Letters*, 27:689–692, 2000. doi: 10.1029/1999GL010928.

Juraj Pálenik, Thomas Spengler, and Helwig Hauser. IsoTrotter: Visually guided empirical modelling of atmospheric convection. *IEEE Transactions on Visualization and Computer Graphics*, 27(2):775–784, 2021. doi: 10.1109/TVCG.2020.3030389.

Mathias W. Rotach and Dino Zardi. On the boundary-layer structure over highly complex terrain: key findings from MAP. *Quarterly Journal of the Royal Meteorological Society*, 133:937–948, 2007. doi: 10.1002/qj.71.

Mathias W. Rotach, Pierluigi Calanca, Giovanni Graziani, Joachim Gurtz, Douw G. Steyn, Roland Vogt, Marco Andretta, Andreas Christen, Stanislaw Cieslik, Richard Connolly, Stephan F. J. De Wekker, Stefano Galmarini, Evgeny N. Kadygrov, Vladimir Kadygrov, Eugene Miller, Bruno Neininger, Magdalena Rucker, Eva van Gorsel, Heinz Weber, Alexandra Weiss, and Massimiliano Zappa. Turbulence structure and exchange processes in an Alpine valley: the Riviera project. *Bulletin of the American Meteorological Society*, 85:1367–1385, 2004. doi: 10.1175/BAMS-85-9-1367.

Juerg Schmidli. Daytime heat transfer processes over mountainous terrain. *Journal of the Atmospheric Sciences*, 70:4041–4066, 2013. doi: 10.1175/JAS-D-13-083.1.

Stefano Serafin, Bianca Adler, Joan Cuxart, Stephan F. J. De Wekker, Alexander Gohm, Branko Grisogono, Norbert Kalthoff, Daniel J. Kirshbaum, Mathias W. Rotach, Jürg Schmidli, Ivana Stiperski, Željko Večenaj, and Dino Zardi. Exchange processes in the atmospheric boundary layer over mountainous terrain. *Atmosphere*, 9(3):102, 2018. doi: 10.3390/atmos9030102.

Reinhold Steinacker. Area-height distribution of a valley and its relation to the valley wind. *Contributions to Atmospheric Physics*, 57:64–71, 1984.

Edmund K. Stone and Malcolm Kitchen. Introducing an approach for extracting temperature from aircraft GNSS and pressure altitude reports in ADS-B messages. *Journal of Atmospheric and Oceanic Technology*, 32:736–743, 2015. doi: 10.1175/JTECH-D-14-00192.1.

Jelle Treep, Gil Bohrer, Judy Shamoun-Baranes, Olivier Duriez, Renato Prata de Moraes Frasson, and Willem Bouten. Using high-resolution GPS tracking data of bird flight for meteorological observations. *Bulletin of the American Meteorological Society*, 97(6):951–961, 2016. doi: 10.1175/BAMS-D-14-00234.1.

Alfred Ultsch. Swarm data mining for the fine structure of thermals. *Technical Soaring*, 36(4): 102–111, 2012.

Johannes S. Wagner, Alexander Gohm, and Mathias W. Rotach. Influence of along-valley terrain heterogeneity on exchange processes over idealized valleys. *Atmospheric Chemistry and Physics*, 15:6589–6603, 2015. doi: 10.5194/acp-15-6589-2015.

Andreas P. Weigel, Fotini K. Chow, Mathias W. Rotach, Robert L. Street, and Ming Xue. High-resolution large-eddy simulations of flow in a steep Alpine valley. Part II: Flow structure and heat budgets. *Journal of Applied Meteorology and Climatology*, 45:87–107, 2006.

C. David Whiteman. *Mountain Meteorology: Fundamentals and Applications*. Oxford University Press, New York, 2000.

XContest. XContest, 2026. URL `https://www.xcontest.org`. Accessed 2026-10-06.